NANO LETTERS

Letter

pubs.acs.org/NanoLett

Coupling Graphene Mechanical Resonators to Superconducting Microwave Cavities

P. Weber,[†] J. Güttinger,*[,†] I. Tsioutsios, D. E. Chang, and A. Bachtold

ICFO-Institut de Ciencies Fotoniques, Mediterranean Technology Park, 08860 Castelldefels, Barcelona, Spain

Supporting Information

ABSTRACT: Graphene is an attractive material for nanomechanical devices because it allows for exceptional properties, such as high frequencies, quality factors, and low mass. An outstanding challenge, however, has been to obtain large coupling between the motion and external systems for efficient readout and manipulation. Here, we report on a novel approach, in which we capacitively couple a high-Q graphene mechanical resonator ($Q \approx 10^5$) to a superconducting microwave cavity. The initial devices exhibit a large single-photon coupling of ~10 Hz. Remarkably, we can electrostatically change the graphene equilibrium position and thereby tune the single photon coupling, the mechanical resonance frequency, and the sign and magnitude of the observed Duffing nonlinearity. The strong tunability opens up new possibilities, such as the tuning of the optomechanical coupling strength on a time scale faster than the inverse of the cavity line width. With realistic improvements, it should be possible to enter the regime of quantum optomechanics.

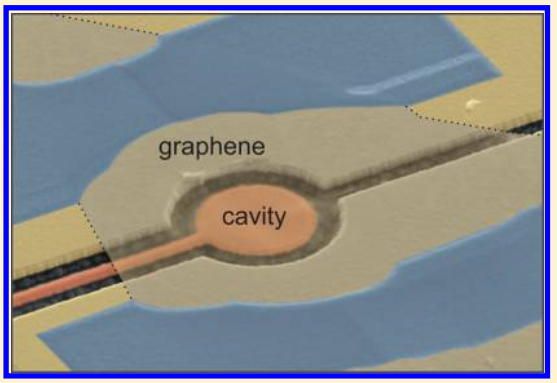

KEYWORDS: *Optomechanics, graphene, mechanical resonator, NEMS, cavity readout, Duffing oscillator*

Mechanical resonators based on individual nanotubes and graphene flakes have outstanding properties. Their masses are ultralow, their quality factors can be remarkably high, the resonance frequencies are widely tunable, and their equilibrium positions can be varied by a large amount. As a result, the resonators can be used as sensors of mass[1,2] and force[3−5] with unprecedented sensitivities, and they can be employed as parametric amplifiers[6] and as tunable oscillators.[6−8] Thus far, all these scientific applications are accomplished in the classical regime.

Reaching the quantum regime with mechanical resonators has attracted considerable interest.[9,10] So far, three groups have been successful in this quest by demonstrating that the number of vibrational quanta can be lowered below one.[11−13] These three groups were using different resonators, namely, a piezoelectric resonator, a superconducting resonator, and an opto-mechanical crystal. There is now an intense effort from the community to develop new types of opto-mechanical and electro-mechanical devices, the goal being to explore new scientific and technological applications when these devices will enter the quantum regime. This includes levitating particles,[14−16] optically trapped cantilevers,[17] and heavy pillars[18] to test the foundations of quantum mechanics; metal coated silicon nitride membranes to coherently convert radio frequency photons to visible photons;[19,20] and microdisks and nanopillars to boost the single-photon coupling and to enter the ultra strong coupling regime.[21,22] In this context, the unique properties of nanotube and graphene resonators are very interesting.

Although nanotubes and graphene have exceptional properties, an outstanding challenge in approaching the quantum regime has been the development of efficient coupling to external elements, which would enable motional readout and manipulation. For example, while graphene has been coupled to an optical cavity,[23] the 2.3% optical absorption of graphene makes it extremely challenging to reach the quantum regime, due to heating of the graphene and quenching of the optical cavity finesse. Here, we employ a different strategy, which is to couple the mechanical resonator capacitively to a superconducting cavity.[12,24−28] This is a promising approach with graphene resonators, because the two-dimensional shape of graphene is ideal for large capacitive coupling.

In this work we report on the integration of a circular graphene resonator with a superconducting microwave cavity. We use a transfer technique to precisely position a high-quality exfoliated graphene flake with respect to a predefined superconducting cavity. We develop a reliable method to reduce the separation between the graphene membrane and the cavity by tightly clamping the graphene sheet in between a support electrode and a cross-linked poly(methyl methacrylate) (PMMA) structure. We show that this technique allows us to improve the mechanical stability and to achieve high mechanical quality factors. By pumping the cavity on a motional sideband, we are able to sensitively readout the

Received: March 7, 2014
Revised: April 18, 2014
Published: April 18, 2014

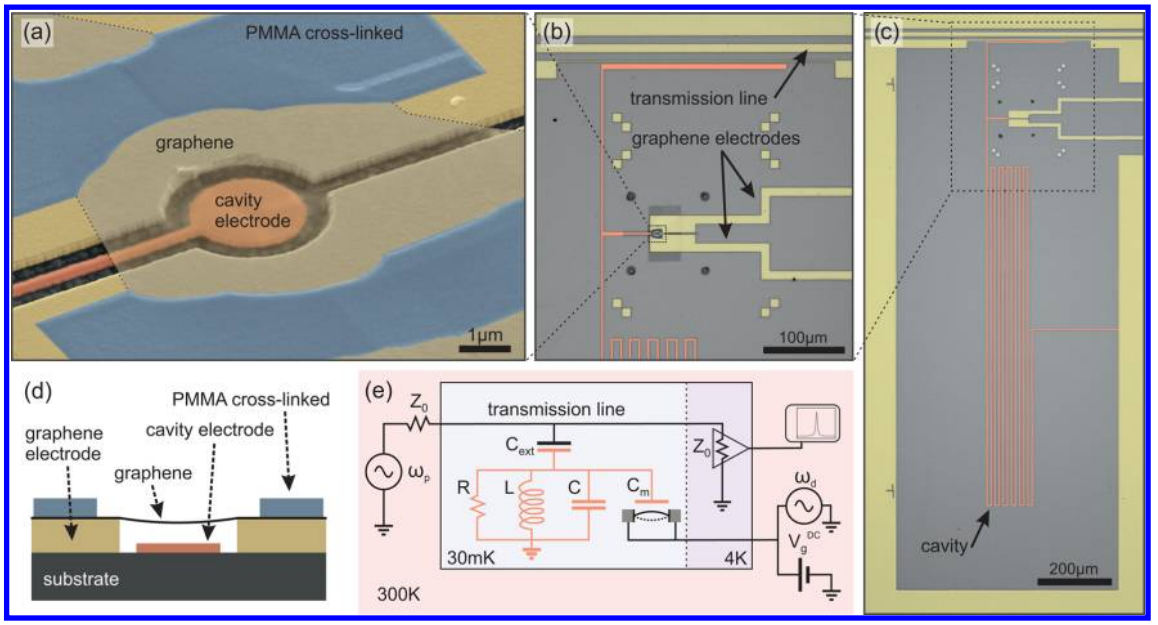

Figure 1. (a) False color SEM image of a circular graphene resonator capacitively coupled to a cavity electrode. The graphene sheet is clamped in between cross-linked PMMA and graphene support electrodes. (b,c) Optical microscope images of the superconducting cavity, the two electrodes contacting the graphene flake, and the capacitively coupled transmission line. (d) Schematic cross-section of the mechanical resonator and the cavity counter electrode. (e) Schematic of the measurement circuit. A coherent pump field at ω_p is applied to the transmission line. The graphene mechanical resonator is driven by a field at ω_d and a constant voltage V_g^{DC}. The microwave signal from the cavity is amplified at 4 K with a HEMT amplifier and recorded at room temperature with a spectrum analyzer. The impedance Z_0 is 50 Ω.

graphene motion. Importantly, by applying a constant voltage V_g^{DC} to the graphene, the properties of the optomechanical device can be dramatically tuned. Namely, large static forces can be produced, allowing to tune the steady-state displacement, the mechanical resonance frequency, the optomechanical coupling, and the mechanical nonlinearities. Such a tunability cannot be achieved in other opto-mechanical systems.

Our device (see Figure 1a–d) consists of a superconducting microwave cavity, modeled as an LC-circuit with angular frequency $\omega_c = 1/(LC_{tot})^{1/2} \approx 6.7$ GHz, capacitance $C_{tot} \approx 90$ fF, inductance $L \approx 6.3$ nH, and characteristic impedance $Z_c = (L/C_{tot})^{1/2} \approx 260$ Ω. The total capacitance $C_{tot} = C + C_{ext} + C_m(z)$ effectively consists of a cavity capacitance $C \approx 85$ fF, a contribution $C_{ext} \approx 5$ fF from the external feedline, and importantly, a contribution $C_m(z) \approx 0.3–0.4$ fF that depends on the graphene position z, which arises from the graphene acting as a moving capacitor plate. A small displacement z therefore produces a shift in ω_c quantified by the optomechanical coupling $G_0 = \partial\omega_c/\partial z$. As a result, the interaction between the mechanical resonator and the superconducting cavity can be described by the Hamiltonian $H_{int} = \hbar G_0 n_p z$ with n_p the number of pump photons in the cavity.[12] The characteristic coupling at the level of the zero-point motion $z_{zp} = (\hbar/2m_{eff}\omega_m)^{1/2}$ is given by the so-called single-photon coupling $g_0 = G_0 z_{zp}$, with m_{eff} the effective mass and $\omega_m/2\pi$ the resonance frequency of the mechanical mode of interest. Central to this work is (i) that the low mass of graphene boosts z_{zp} and thus g_0, and (ii) that C_m and g_0 can be tuned electrostatically with V_g^{DC}.

We start with engineering considerations in order to maximize the coupling g_0. When describing C_m by a plate capacitor and noting that $C \gg C_{ext} \gg C_m(z)$ in our device, we have $g_0 \approx (\omega_c/2C)(\partial C_m(z)/\partial z) z_{zp} \propto (A/\omega_m)^{1/2}\omega_c/Cd^2$ using $\partial C_m(z)/\partial z \propto A/d^2$ and $z_{zp} \propto 1/(A\omega_m)^{1/2}$. Here A is the area of the suspended graphene region and d is the separation between the graphene membrane and its cavity counter electrode. In order to optimize the coupling g_0, it is crucial to minimize both C and d. To this end, we utilize a narrow cavity conductor structured in a meander to increase L, while minimizing the capacitance for a given ω_c. In order to be able to tune d with V_g^{DC}, we use a cavity that is shorted to ground on one side, allowing for a well-defined electrical DC potential. The fundamental mode of the cavity is a quarter-wavelength standing wave, with a voltage node at the shorted end and the largest voltage oscillation amplitudes at the open end. The graphene membrane is coupled close to the open end of the cavity to harness the largest cavity fields (see Figure 1b,c).[24,29,30] Using this geometry, we achieve a cavity capacitance of $C \approx 90$ fF. This compares favorably with $C = 18$ fF–1 pF in previous studies.[12,24–28] Note that the lowest values for C have been achieved in closed-loop cavities, where the mechanical capacitance is incorporated between the two ends of a half-wavelength cavity.[12,27] In this geometry the two electrodes of the mechanical capacitance are shorted over the cavity, so that no static DC potential can be applied. Compared to the capacitance of a gated half-wavelength cavity,[31–33] the capacitance of a quarter-wavelength cavity is lowered by a factor of 2.

In order to detect the vibrations of the graphene resonator, we couple the open-end of the superconducting cavity to a microwave transmission line through the capacitance C_{ext}. The transmission line is used to pump the superconducting cavity at frequency $\omega_p/2\pi$ with input power $P_{p,in}$. The transmission line is also employed to measure the output power P_{out} of the cavity at frequency $\omega_c/2\pi$. P_{out} is amplified at 4 K by a high-electron-mobility transistor (HEMT) with a noise temperature of about 2 K and measured in a spectrum analyzer (see schematic in Figure 1e and Supporting Information).

We use a graphene resonator with a circular shape. This geometry improves the attachment of the graphene sheet to its

dx.doi.org/10.1021/nl500879k | Nano Lett. 2014, 14, 2854–2860

support when compared to the doubly clamped resonator geometry. As further discussed below, a strong attachment of the graphene to its support is crucial to be able to lower d. Another advantage of circular graphene resonators over doubly clamped resonators is that the quality factor tends to be larger.[34] In addition, the mechanical eigenmodes of circular resonators are well-defined.[34,35] In particular, it avoids the formation of modes localized at the edges, which were observed in doubly clamped resonators.[36]

To fabricate the devices, we start by carving out the superconducting cavity structure from a 200 nm thick sputtered niobium (Nb) film by ion milling and reactive ion etching (see Supporting Information). We employ a PMMA supported transfer technique pioneered at Columbia[37] to position graphene flakes on the superconducting cavity structure. For this, we exfoliate graphene sheets from large graphite crystals onto a silicon (Si) chip covered by a polymer film consisting of 100 nm poly(vinyl alcohol) (PVA) and 200 nm PMMA 495 K. The thickness of the PVA/PMMA film is optimized to give the largest optical contrast of graphene flakes in an optical microscope. In particular, it allows to calibrate the number of layers of the graphene flake.[38,39] The solvability of PVA in water is used to separate the Si chip from the PMMA with the graphene. Using a brass slide with a volcano-shaped hole, the membrane is fished from the water and dried on a hot plate. When drying, the PMMA membrane gets uniformly stretched across the volcano hole. By mounting the slide upside down into a micromanipulator, the graphene sheet can be aligned and transferred onto the prepatterned superconducting cavity structure, as illustrated in Figure 2a. To improve the attachment of the graphene flake to its support, it was shown that it is important to clamp the graphene membrane on the two sides of its surface.[40] For this, we cross-link part of the transferred PMMA with a 10 000 μC/cm^2 electron beam dose (Figure 2b). The unexposed PMMA is removed in 80 °C hot N-methyl-2-pyrrolidone (NMP), followed by critical point drying of the device. As a result, the graphene is firmly sandwiched between the support electrode and the cross-linked PMMA (Figure 2c,d). Using this technique the graphene sheet is less likely to collapse against its counter electrode. This allows us to increase the success yield of the device fabrication. We have successfully lowered the separation to d = 85 nm for a 3.5 μm diameter graphene resonator, which is equal to the best diameter/separation ratio of $2R/d$ = 40 reported so far for graphene resonators.[41] In addition, the strong attachment between the graphene and its support allows us to electrostatically tune the equilibrium position by a large amount (see below).

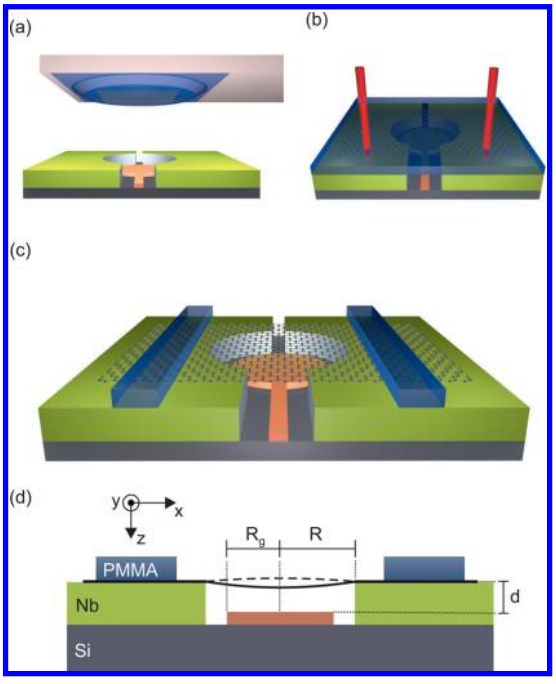

Figure 2. Fabrication process for PMMA-clamped graphene mechanical resonator. (a) Transfer of graphene with PMMA (blue) onto predefined structure (yellow/green, gray). (b) Cross-linking part of the transferred PMMA by electron-beam overexposure (red). (c) Schematic of the final device. (d) Cross-section of the device.

In this letter we present results measured at 30 mK for two different graphene devices, hereafter called devices A and B. Device A is a three layer graphene resonator with radius R = 1.75 μm and with d = 95 nm. The number of layers is determined from optical contrast measurements.[38,39] The radius of the counter electrode is R_g = 1.1 μm (see Figure 2d). Device B is a four layer graphene resonator with the same membrane radius, d = 135 nm and R_g = 1.25 μm.

The principle of mechanical vibration readout is analogous to Stokes and anti-Stokes Raman scattering. By pumping the cavity at ω_p, sidebands in energy are created at $\omega_p \pm \omega_m$ due to the coupling of the photons with the mechanical motion. If the pump is detuned such that the upper sideband frequency is matched with the cavity resonance frequency $\omega_c = \omega_p + \omega_m$ (see Figure 3a), the anti-Stokes scattering is resonantly enhanced. Then, the rate of the anti-Stokes scattering per phonon is given by $\Gamma_{opt} \approx 4n_p g_0^2/\kappa$, with $n_p \propto P_{p,in}(\omega_p)$ the number of photons in the cavity. We drive the graphene resonator by applying a constant voltage V_g^{DC} and an oscillating voltage with amplitude V_g^{AC} at a frequency $\omega_d/2\pi$ close to $\omega_m/2\pi$ so that $\omega_d = \omega_c - \omega_p$. As a result, the graphene resonator vibrates at $z(t) = \hat{z}\cos(\omega_d t + \phi)$ with ϕ the phase difference between the displacement and the driving force. The output power at ω_c is

$$P_{out} = P_{p,in}\frac{\kappa_{ext}^2}{\kappa^2 + 4(\omega_c - \omega_p)^2}4\frac{g_0^2}{\kappa^2}\frac{\langle z(t)^2\rangle}{2z_{zp}^2} \quad (1)$$

From a transmission measurement of the feedline we readily get the resonance frequency of the cavity $\omega_c/2\pi$ = 6.73 GHz and the total line width $\kappa/2\pi = \kappa_{ext}/2\pi + \kappa_{int}/2\pi$ = 15.2 MHz with $\kappa_{ext}/2\pi$ = 2 MHz the coupling rate of the superconducting cavity to the feedline and $\kappa_{int}/2\pi$ = 13.2 MHz the internal loss rate of the cavity. A detailed analysis of the circuit, which includes a resistance to describe the losses in the graphene flake and the DC connections, shows that this additional resistance contributes roughly 20% to κ_{int} (see Supporting Information). The high value of κ_{int} is attributed to the contaminations and imperfections of the cavities. Indeed, we tested the cavity of devices A and B at T = 4.2 K before the transfer of the graphene flakes, and we observed larger κ_{int} than what we usually observe in devices processed in the same way.

Figure 3b,c shows the resonance of the driven vibrations for the fundamental modes of devices A and B. Modes at higher frequencies are observed as well, but they are hardly detectable. For device A we extract the mechanical quality factor $Q_m = \omega_m/\gamma_m \approx 100\,000$ from the line width of the resonance $\gamma_m/2\pi$ = 575 Hz. This Q_m is comparable to the largest values reported thus far for graphene resonators,[42] showing that our fabrication

dx.doi.org/10.1021/nl500879k | Nano Lett. 2014, 14, 2854−2860

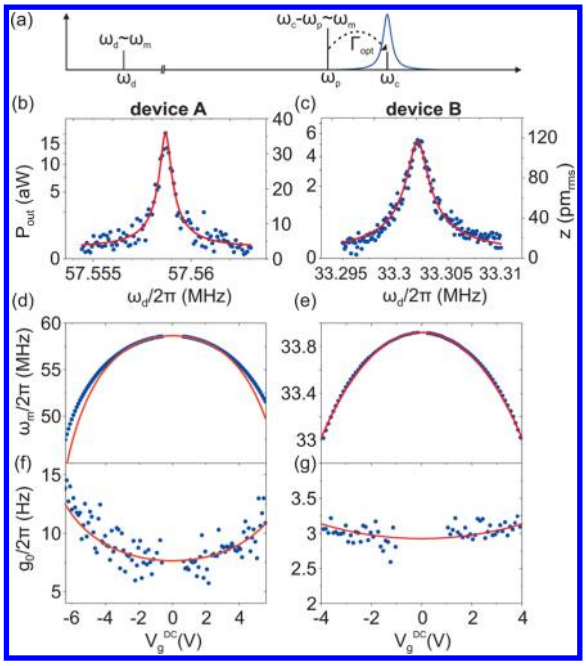

Figure 3. (a) Measurement scheme: If the pump frequency is detuned such that $\omega_p = \omega_c - \omega_m$, anti-Stokes scattering with phonons at rate Γ_{opt} leads to a detectable photon population at ω_c. (b,c) Sideband measurement of the mechanical motion for device *A* with $V_g^{DC} = -2.894$ V and $V_g^{AC} = 190$ nV, and for device *B* with $V_g^{DC} = 3.405$ V and $V_g^{AC} = 4.3$ μV. Red lines are Lorentzian fits to the data, which yield a mechanical quality factor of $Q_m = 100\,000$ in device *A* and $Q_m = 17\,700$ in device *B*. The calculated motional root-mean-square amplitude *z* is plotted on the right scale. (d,e) Mechanical resonance frequency as a function of V_g^{DC}. We have compensated V_g^{DC} by an offset of 0.434 V for device *A* and 0.395 V for device *B*. In addition to capacitive softening, the static deflection z_s of the resonator toward the cavity counter electrode is considered in order to account for the measurement (red line). (f,g) Single-photon coupling rate $g_0 = G_0 z_{zp}$. By including the static displacement z_s we are able to model the single-photon coupling as a function of V_g^{DC} (red line).

process does provide us with mechanical resonators of excellent quality. We used $n_p = 8000$ photons for this measurement, so that $\Gamma_{opt}/2\pi \approx 0.12$ Hz. With these parameters, the measurement imprecision, estimated to be 2.5 pm/(Hz)$^{1/2}$, is limited by the noise of the low-temperature HEMT amplifier. For comparison, the height of the resonance in the power spectral density of the thermal motion at 30 mK is (7 fm)^2/Hz (see Supporting Information). In device *B* we measure a quality factor of $Q_m = 17\,700$. We attribute this lower Q_m to the fact that the device was imaged in a scanning electron microscope (SEM) before the measurements, where the graphene surface got contaminated by amorphous carbon. This measurement was done with $n_p = 4500$ photons, corresponding to $\Gamma_{opt}/2\pi \approx 0.01$ Hz. If we further increase the pump power we observe a reduction of the quality factor. We attribute this reduction of Q_m to Joule heating in the graphene flake. A rough estimate of the heating can be made by measuring the quality factor as a function of the temperature of the cryostat. From this comparison, $n_p = 10^6$ corresponds, for instance, to a temperature of about 200 mK (see Supporting Information).

The resonance frequency decreases upon increasing $|V_g^{DC}|$ (see Figure 3d,e). This reduction of the resonance frequency has been observed previously in graphene resonators under tension.[42−44] This softening of the resonator is attributed to the change of the restoring potential of the resonator by the capacitive energy.[42−45] We model the mechanical resonator with a circular membrane under tension[46] to quantify the observed dependence. When neglecting static deflection, the frequency dependence is given by

$$\omega_m(V_g^{DC}) = \sqrt{\frac{4.92Eh\varepsilon}{m_{eff}} - \frac{0.271}{m_{eff}}\frac{\varepsilon_0\pi R_g^{\,2}}{d^3}(V_g^{DC})^2} \quad (2)$$

with ε the strain in the graphene sheet, $E \approx 1$ TPa the Young's modulus of graphite, $h = n_g \times 0.34$ nm the graphene thickness, n_g the number of graphene layers[3,43] and $m_{eff} = 0.27\pi R^2\rho_{2D}$ the effective mass of the fundamental mode (see Supporting Information). The two-dimensional mass density $\rho_{2D} = \eta n_g \rho_{graphene}$ includes the graphene mass density $\rho_{graphene} = 7.6 \times 10^{-19}$ kg/μm^2 and a correction factor $\eta \geq 1$ to account for contamination on the graphene surface. From a fit of eq 2 to the measurements around $V_g^{DC} = 0$ (in Figure 3d,e), we extract $m_{eff} = 13 \times 10^{-18}$ kg and $\varepsilon = 0.036\%$ for device *A*, and $m_{eff} = 36 \times 10^{-18}$ kg and $\varepsilon = 0.024\%$ for device *B*. The obtained mass is $\eta = 2.2$ times larger than the total graphene mass for device *A* and $\eta = 4.5$ times larger for device *B*. The larger η for device *B* might be attributed to the amorphous carbon deposited during SEM inspection. The tension is intermediate compared to previous measurements, where ε ranges from 0.002% to 1%.[3,34,42,47]

In order to account for the variation of ω_m for large V_g^{DC} in Figure 3d,e, the static deflection of the graphene sheet toward the cavity counter electrode has to be considered. The static displacement of the center of the membrane z_s is given by

$$z_s = \frac{\varepsilon_0 R_g^{\,2}}{8Eh\varepsilon d^2}(V_g^{DC})^2 = c_s(V_g^{DC})^2 \quad (3)$$

for small displacement compared to *d*. Although the renormalization of the mechanical frequency due to static displacement cannot be solved exactly, as an approximation we can include z_s in eq 2 using $d = d_0 - z_s$, with d_0 the separation for $V_g^{DC} = 0$. We get a good agreement for $\omega_m(V_g^{DC})$ between the measurements and theory without any fitting parameter over the V_g^{DC} range shown in Figure 3d,e. The effect of z_s on the shift in ω_m is 42% at $V_g^{DC} = -6$ V for device *A* and 10% at $V_g^{DC} = 4$ V for device *B*. The expected variation of z_s is plotted in Figure 4a.

The softening of the graphene resonator becomes enormous upon further increasing V_g^{DC}, with a reduction of ω_m by a factor

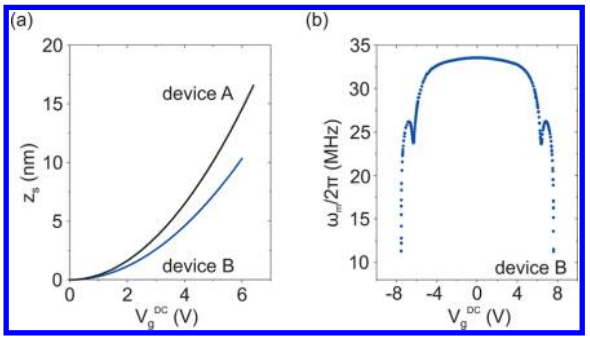

Figure 4. (a) Static displacement of the center of the membrane calculated from eq 3 with constants $c_s = 0.405$ nm/V^2 for device *A* and $c_s = 0.287$ nm/V^2 for device *B*. (b) Mechanical resonance frequency as a function of V_g^{DC} for device *B*.

dx.doi.org/10.1021/nl500879k | Nano Lett. 2014, 14, 2854−2860

of 3 down to ~10 MHz as shown in Figure 4b for device *B*. This reduction of ω_m is large compared to that measured in previous works.[43−45] Such a large reduction is expected when the capacitive force becomes comparable to the restoring force of the resonator. When the two forces are equal, ω_m drops to zero and the resonator collapses against the counter electrode.[48] Even though further work is needed to understand the quantitative dependence of ω_m on V_g^{DC}, it reveals that the graphene resonators we fabricate can bend by a large amount without being ripped apart due to the large induced strain and without sliding with respect to the anchor electrodes.

The static displacement of the graphene sheet also changes the resonance frequency of the microwave cavity upon varying V_g^{DC}. As the graphene moves closer to the cavity counter electrode, the total capacitance of the cavity increases, so that the cavity frequency decreases. For $\Delta V_g^{DC} = 6$ V the decrease is $\Delta\omega_c/2\pi = 2$ MHz in device *A*. The measured $\Delta\omega_c$ agrees well with the shift expected from the static displacement (see Supporting Information).

Our device layout allows us to get large couplings g_0 between the mechanical resonator and the superconducting cavity (Figure 3f,g). We extract g_0 from the measurements of the response of driven vibrations at $\omega_d = \omega_m$ using eq 1 where $\langle z(t)^2\rangle = [\partial_z C_m \cdot V_g^{DC} V_g^{AC} Q_m/(m_{eff}\omega_m^2)]^2$. Remarkably, g_0 gets larger upon increasing $|V_g^{DC}|$ for device *A*. This tunability of g_0 is attributed to the static deflection of the graphene sheet. When incorporating the effect of the static displacement into C_m, we get a good agreement between the expected $g_0 = (\omega_c/2C)(\partial C_m(z)/\partial z)z_{zp}$ and the measurements, using $C = 75$ fF and 100 fF for devices *A* and *B*, respectively (red lines in Figure 3f,g). These values of *C* agree well with $C = 90$ fF estimated from simulations. The obtained coupling rates g_0 compare favorably with previous experiments carried out with mechanical resonators made from other materials. Indeed, the coupling was $g_0/2\pi \approx 1$ Hz in works with cavity geometries similar to ours.[26,28,49] Larger values were achieved with closed-loop cavities ($g_0/2\pi = 40$ and 210 Hz), but this geometry does not allow one to apply V_g^{DC} between the mechanical resonator and a counter electrode as discussed above.[12,27]

Now, we investigate how the strong tunability of the graphene equilibrium position affects the nonlinear response of the mechanical resonator. For this, we measure P_{out} as a function of ω_d as in Figure 3b,c in order to obtain the response of the vibrational amplitude $\hat{z}(\omega_d)$ for large driving forces at different V_g^{DC} (Figure 5a−c). Interestingly, we are able to tune the sign of the Duffing nonlinearity from a hardening behavior at low V_g^{DC} (Figure 5a) to a softening behavior at high V_g^{DC} (Figure 5c). At an intermediate V_g^{DC} of about 3.4 V, we are able to cancel the Duffing nonlinearity, that is, the resonant frequency remains roughly constant upon varying the driving force (Figure 5b). We quantify the Duffing nonlinearity from the critical displacement amplitude $\hat{z}_{crit}$ above which the response becomes bistable. For a Duffing resonator with linear damping, the effective Duffing constant α_{eff} is related to $\hat{z}_{crit}$ by $\alpha_{eff} = (1.54 m_{eff}\omega_m^2/(Q_m\hat{z}_{crit}))$.[50] Figure 5d shows that α_{eff} is positive at low V_g^{DC} and becomes negative at large V_g^{DC}. This dependence can be attributed to the symmetry breaking of the mechanical motion induced by static deflection,[51,52] which reads

$$\alpha_{eff} \approx \alpha_0 - \frac{10}{m_{eff}\omega_m^2}\alpha_0^2 z_s^2 \quad (4)$$

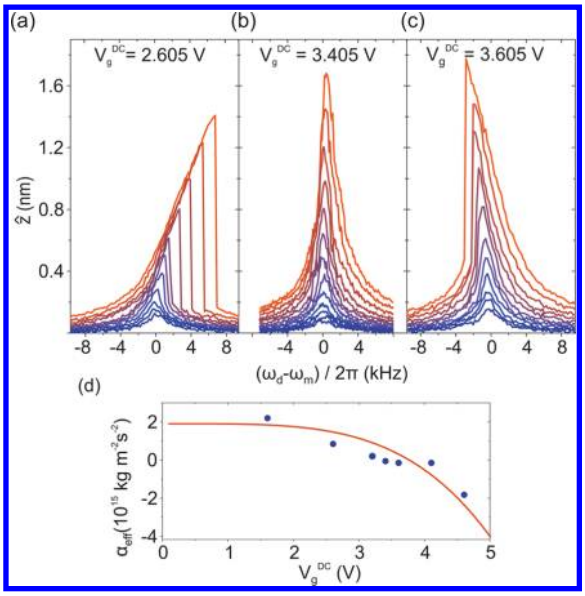

Figure 5. (a−c) Dependence of the vibrational amplitude $\hat{z}$ in device *B* on the drive frequency for different V_g^{AC} in each plot. In panels a and c, $V_g^{AC} = 3-31$ μV; in panel b, $V_g^{AC} = 1.9-31$ μV. The onset of bistability is determined to be at $\hat{z}_{crit} = 360$ pm (a) and at $\hat{z}_{crit} = 900$ pm (c). (d) Effective Duffing parameter α_{eff} as a function of V_g^{DC}. The red line is a plot of eq 4 with $c_s = 0.65$ nm/V^2 and $\alpha_0 = 1.9 \times 10^{15}$ kg m^{-2} s^{-2}.

where α_0 is the Duffing constant when $V_g^{DC} = 0$; α_0 could have a geometrical origin.[50] The fit of eq 4 to the measurement yields $c_s = 0.65$ nm/V^2 and $\alpha_0 = 1.9 \times 10^{15}$ kg m^{-2} s^{-2} (red line in Figure 5d). This value of c_s is consistent with that expected from eq 3. The sign change of the Duffing nonlinearity due to static deformation is a unique property of graphene and nanotube resonators.[53]

The prospects to reach the quantum regime with graphene resonators are promising. For this, it is illustrative to compare the figures of merit achieved here to those reported by Teufel et al.,[12] which demonstrated ground-state cooling with a superconducting cavity. In device *A* of our work, we measure $g_0/2\pi \approx 15$ Hz, $n_p = 8000$, $Q_m = 100\,000$, and $\kappa_{int}/2\pi = 13.2$ MHz, while the parameters of Teufel et al. are $g_0/2\pi \approx 200$ Hz, $n_p = 4000$, $Q_m = 350\,000$, and $\kappa_{int}/2\pi = 40$ kHz. As discussed above, an obvious way to improve κ_{int} is to fabricate cavities with less contamination and imperfections. κ_{int} can then be further reduced by lowering the resistance of the graphene flake. This can be achieved for instance by selecting thicker graphene flakes or electrostatically doping the graphene. Minimizing the graphene resistance, together with increasing the area of the interface between the graphene and the electrodes, is beneficial for diminishing Joule heating at high pump power. In order to increase g_0, we will reduce *d* further by fabrication and graphene pulling. We should reach $g_0/2\pi \approx 250$ Hz with $d = 30$ nm. An alternative route to increase g_0 is to enhance the coupling using a cooper-pair box.[54,55]

In conclusion, we have reported devices where a graphene resonator is coupled to a superconducting cavity. The tunability of these devices, in combination with the large graphene−cavity coupling, constitutes a promising approach to study quantum motion. The large reduction of the resonance frequency of the graphene resonator observed here is interesting to enhance the zero-point motion and to increase the effect of mechanical nonlinearities.[56−58] The tunability of the resonance frequency with V_g^{DC} is suitable for parametric amplification and quantum

dx.doi.org/10.1021/nl500879k | *Nano Lett.* 2014, 14, 2854−2860

squeezing of mechanical states.[59] In these graphene−cavity devices, the opto-mechanical coupling can be varied not only with the number of pump photons but also with V_g^{DC}. Interestingly, the tuning of the coupling with V_g^{DC} can be made faster than that with n_p since the inverse of the cavity line width poses an upper limit on how fast the photon number inside the cavity can be changed. Because the mass of graphene is ultralow, its motion is extremely sensitive to changes in the environment. Therefore, it will be interesting to couple the quantum vibrations of motion to other degrees of freedom, such as electrons and spins.

■ ASSOCIATED CONTENT

Supporting Information

Additional information on the sample fabrication, further characterization measurements, and the derivation of the electrical and mechanical model. This material is available free of charge via the Internet at http://pubs.acs.org.

■ AUTHOR INFORMATION

Corresponding Author

*(J.G.) E-mail: johannes.guettinger@icfo.es.

Author Contributions

†These authors (P.W. and J.G.) contributed equally to this work. P.W., J.G., and I.T. developed the fabrication process. P.W. fabricated the devices with support from J.G. The experimental setup was built up by J.G. with support from P.W. P.W. and J.G. carried out the measurements. J.G. and P.W. analyzed the data with support from A.B. and D.E.C. J.G. and A.B. wrote the manuscript with critical comments from all authors. A.B. and J.G. conceived the experiment and supervised the work.

Notes

The authors declare no competing financial interest.

■ ACKNOWLEDGMENTS

We would like to thank Joel Moser, Gabriel Puebla, Christopher Eichler, Andreas Isacsson, Martin Eriksson, Sara Hellmüller, and Andreas Wallraff for helpful discussions. We gratefully acknowledge Gustavo Ceballos and the ICFO mechanical and electronic workshop for support. We acknowledge support from the European Union through the RODIN-FP7 project, the ERC-carbonNEMS project, the Graphene Flagship (grant agreement 604391), the Spanish state (MAT2012-31338), the Catalan government (AGAUR, SGR).

■ REFERENCES

(1) Chiu, H.-Y.; Hung, P.; Postma, H. W. C. *Nano Lett.* **2008**, *8*, 4342.

(2) Chaste, J.; Eichler, A.; Moser, J.; Ceballos, G.; Rurali, R.; Bachtold, A. *Nat. Nanotechnol.* **2012**, *7*, 301.

(3) Bunch, J. S.; Van Der Zande, A. M.; Verbridge, S. S.; Frank, I. W.; Tanenbaum, D. M.; Parpia, J. M.; Craighead, H. G.; McEuen, P. L. *Science* **2007**, *315*, 490.

(4) Moser, J.; Güttinger, J.; Eichler, A.; Esplandiu, M.; Liu, D.; Dykman, M.; Bachtold, A. *Nat. Nanotechnol.* **2013**, *8*, 493496.

(5) Stapfner, S.; Ost, L.; Hunger, D.; Reichel, J.; Favero, I.; Weig, E. M. *Appl. Phys. Lett.* **2013**, *102*, 151910.

(6) Eichler, A.; Chaste, J.; Moser, J.; Bachtold, A. *Nano Lett.* **2011**, *11*, 2699.

(7) Ayari, A.; Vincent, P.; Perisanu, S.; Choueib, M.; Gouttenoire, V.; Bechelany, M.; Cornu, D.; Purcell, S. T. *Nano Lett.* **2007**, *7*, 2252.

(8) Chen, C.; Lee, S.; Deshpande, V. V.; Lee, G.-H.; Lekas, M.; Shepard, K.; Hone, J. *Nat. Nanotechnol.* **2013**, *8*, 923.

(9) Poot, M.; van der Zant, H. S. *Phys. Rep.* **2012**, *511*, 273.

(10) Aspelmeyer, M.; Kippenberg, T. J.; Marquardt, F. arXiv preprint arXiv:1303.0733, 2013); http://arxiv.org/abs/1303.0733.

(11) OConnell, A. D.; Hofheinz, M.; Ansmann, M.; Bialczak, R. C.; Lenander, M.; Lucero, E.; Neeley, M.; Sank, D.; Wang, H.; Weides, M.; Martinis, J. M.; Cleland, A. N. *Nature* **2010**, *464*, 697.

(12) Teufel, J.; Donner, T.; Li, D.; Harlow, J.; Allman, M.; Cicak, K.; Sirois, A.; Whittaker, J.; Lehnert, K.; Simmonds, R. *Nature* **2011**, *475*, 359363.

(13) Chan, J.; Alegre, T. M.; Safavi-Naeini, A. H.; Hill, J. T.; Krause, A.; Gröblacher, S.; Aspelmeyer, M.; Painter, O. *Nature* **2011**, *478*, 89.

(14) Chang, D. E.; Regal, C. A.; Papp, S. B.; Wilson, D. J.; Ye, J.; Painter, O.; Kimble, H. J.; Zoller, P. *Proc. Natl. Acad. Sci. U.S.A.* **2010**, *107*, 1005.

(15) Kiesel, N.; Blaser, F.; Delić, U.; Grass, D.; Kaltenbaek, R.; Aspelmeyer, M. *Proc. Natl. Acad. Sci. U.S.A.* **2013**, *110*, 14180.

(16) Gieseler, J.; Novotny, L.; Quidant, R. *Nat. Phys.* **2013**, *9*, 806.

(17) Ni, K.-K.; Norte, R.; Wilson, D. J.; Hood, J. D.; Chang, D. E.; Painter, O.; Kimble, H. J. *Phys. Rev. Lett.* **2012**, *108*, 214302.

(18) Kuhn, A. G.; Bahriz, M.; Ducloux, O.; Chartier, C.; Le Traon, O.; Briant, T.; Cohadon, P.-F.; Heidmann, A.; Michel, C.; Pinard, L.; Flaminio, R. *Appl. Phys. Lett.* **2011**, *99*, 121103.

(19) Bagci, T.; Simonsen, A.; Schmid, S.; Villanueva, L.; Zeuthen, E.; Appel, J.; Taylor, J.; Sørensen, A.; Usami, K.; Schliesser, A. *Nature* **2013**, *507*, 81.

(20) Andrews, R.; Peterson, R.; Purdy, T.; Cicak, K.; Simmonds, R.; Regal, C.; Lehnert, K. *Nat. Phys.* **2014**, *10*, 321326.

(21) Ding, L.; Baker, C.; Senellart, P.; Lemaitre, A.; Ducci, S.; Leo, G.; Favero, I. *Phys. Rev. Lett.* **2010**, *105*, 263903.

(22) Yeo, I.; de Assis, P.-L.; Gloppe, A.; Dupont-Ferrier, E.; Verlot, P.; Malik, N. S.; Dupuy, E.; Claudon, J.; Gérard, J.-M.; Auffèves, A.; Nogues, G.; Seidelin, S.; Poizat, J.-Ph.; Arcizet, O.; Richard, M. *Nat. Nanotechnol.* **2013**, *9*, 106.

(23) Barton, R. A.; Storch, I. R.; Adiga, V. P.; Sakakibara, R.; Cipriany, B. R.; Ilic, B.; Wang, S. P.; Ong, P.; McEuen, P. L.; Parpia, J. M.; Craighead, H. G. *Nano Lett.* **2012**, *12*, 4681.

(24) Regal, C.; Teufel, J.; Lehnert, K. *Nat. Phys.* **2008**, *4*, 555.

(25) Hertzberg, J.; Rocheleau, T.; Ndukum, T.; Savva, M.; Clerk, A.; Schwab, K. *Nat. Phys.* **2009**, *6*, 213.

(26) Rocheleau, T.; Ndukum, T.; Macklin, C.; Hertzberg, J.; Clerk, A.; Schwab, K. *Nature* **2010**, *463*, 72.

(27) Massel, F.; Heikkilä, T.; Pirkkalainen, J.-M.; Cho, S.; Saloniemi, H.; Hakonen, P.; Sillanpää, M. *Nature* **2011**, *480*, 351.

(28) Zhou, X.; Hocke, F.; Schliesser, A.; Marx, A.; Huebl, H.; Gross, R.; Kippenberg, T. *Nat. Phys.* **2013**, *9*, 179.

(29) Day, P. K.; LeDuc, H. G.; Mazin, B. A.; Vayonakis, A.; Zmuidzinas, J. *Nature* **2003**, *425*, 817.

(30) Teufel, J.; Donner, T.; Castellanos-Beltran, M.; Harlow, J.; Lehnert, K. *Nat. Nanotechnol.* **2009**, *4*, 820.

(31) Delbecq, M. R.; Schmitt, V.; Parmentier, F. D.; Roch, N.; Viennot, J. J.; Fève, G.; Huard, B.; Mora, C.; Cottet, A.; Kontos, T. *Phys. Rev. Lett.* **2011**, *107*, 256804.

(32) Frey, T.; Leek, P. J.; Beck, M.; Blais, A.; Ihn, T.; Ensslin, K.; Wallraff, A. *Phys. Rev. Lett.* **2012**, *108*, 046807.

(33) Petersson, K.; McFaul, L.; Schroer, M.; Jung, M.; Taylor, J.; Houck, A.; Petta, J. *Nature* **2012**, *490*, 380.

(34) Barton, R. A.; Ilic, B.; van der Zande, A. M.; Whitney, W. S.; McEuen, P. L.; Parpia, J. M.; Craighead, H. G. *Nano Lett.* **2011**, *11*, 1232.

(35) Eriksson, A.; Midtvedt, D.; Croy, A.; Isacsson, A. *Nanotechnology* **2013**, *24*, 395702.

(36) Garcia-Sanchez, D.; van der Zande, A. M.; Paulo, A. S.; Lassagne, B.; McEuen, P. L.; Bachtold, A. *Nano Lett.* **2008**, *8*, 1399.

(37) Dean, C.; Young, A.; Meric, I.; Lee, C.; Wang, L.; Sorgenfrei, S.; Watanabe, K.; Taniguchi, T.; Kim, P.; Shepard, K.; Hone, J. *Nat. Nanotechnol.* **2010**, *5*, 722.

(38) Blake, P.; Hill, E. W.; Castro Neto, A. H.; Novoselov, K. S.; Jiang, D.; Yang, R.; Booth, T. J.; Geim, A. K. *Appl. Phys. Lett.* **2007**, *91*, 063124.

(39) Ni, Z. H.; Wang, H. M.; Kasim, J.; Fan, H. M.; Yu, T.; Wu, Y. H.; Feng, Y. P.; Shen, Z. X. *Nano Lett.* **2007**, *7*, 2758.
(40) Bao, W.; Myhro, K.; Zhao, Z.; Chen, Z.; Jang, W.; Jing, L.; Miao, F.; Zhang, H.; Dames, C.; Lau, C. N. *Nano Lett.* **2012**, *12*, 5470.
(41) Lee, S.; Chen, C.; Deshpande, V. V.; Lee, G.-H.; Lee, I.; Lekas, M.; Gondarenko, A.; Yu, Y.- J.; Shepard, K.; Kim, P.; Hone, J. *Appl. Phys. Lett.* **2013**, *102*, 153101.
(42) Eichler, A.; Moser, J.; Chaste, J.; Zdrojek, M.; Wilson-Rae, I.; Bachtold, A. *Nat. Nanotechnol.* **2011**, *6*, 339.
(43) Chen, C.; Rosenblatt, S.; Bolotin, K.; Kalb, W.; Kim, P.; Kymissis, I.; Stormer, H.; Heinz, T.; Hone, J. *Nat. Nanotechnol.* **2009**, *4*, 861.
(44) Song, X.; Oksanen, M.; Sillanpää, M. A.; Craighead, H.; Parpia, J.; Hakonen, P. J. *Nano Lett.* **2011**, *12*, 198.
(45) Kozinsky, I.; Postma, H. W. C.; Bargatin, I.; Roukes, M. L. *Appl. Phys. Lett.* **2006**, *88*, 253101.
(46) Landau, L. D.; Lifshitz, E.; Sykes, J.; Reid, W.; Dill, E. H. *Theory of Elasticity: Course of Theoretical Physics*, 2nd ed.; Pergamon Press: Oxford, U.K., 1970; Vol. 7.
(47) Chen, C.; Hone, J. *Proc. IEEE* **2013**, *101*, 1766.
(48) Sillanpää, M. A.; Khan, R.; Heikkilä, T. T.; Hakonen, P. J. *Phys. Rev. B* **2011**, *84*, 195433.
(49) Teufel, J. D.; Harlow, J. W.; Regal, C. A.; Lehnert, K. W. *Phys. Rev. Lett.* **2008**, *101*, 197203.
(50) Lifshitz, R.; Cross, M. *Reviews of Nonlinear Dynamics and Complexity* **2008**, *1*, 1.
(51) Younis, M.; Nayfeh, A. *Nonlinear Dynamics* **2003**, *31*, 91.
(52) Eichler, A.; Moser, J.; Dykman, M.; Bachtold, A. *Nat. Commun.* **2013**, *4*, 2843.
(53) Eichler, A.; del Álamo Ruiz, M.; Plaza, J. A.; Bachtold, A. *Phys. Rev. Lett.* **2012**, *109*, 025503.
(54) Heikkilä, T. T.; Massel, F.; Tuorila, J.; Khan, R.; Sillanpää, M. A. arXiv preprint arXiv:1311.3802, 2013; http://arxiv.org/abs/1311.3802.
(55) Rimberg, A.; Blencowe, M.; Armour, A.; Nation, P. arXiv preprint arXiv:1312.7521, 2013; http://arxiv.org/abs/1312.7521.
(56) Voje, A.; Kinaret, J. M.; Isacsson, A. *Phys. Rev. B* **2012**, *85*, 205415.
(57) Rips, S.; Hartmann, M. J. *Phys. Rev. Lett.* **2013**, *110*, 120503.
(58) Rips, S.; Wilson-Rae, I.; Hartmann, M. J. *Phys. Rev. A* **2014**, *89*, 013854.
(59) Lü, X. Y.; Liao, J. Q.; Tian, L.; Nori, F. arXiv preprint arXiv:1403.0049, 2014; http://arxiv-web3.library.cornell.edu/abs/1403.0049.
(60) Song, X.; Oksanen, M.; Li, J.; Hakonen, P. J.; Sillanpä, M. A. Graphene optomechanics realized at microwave frequencies; arXiv preprint arXiv:1403.2965, 2014; http://arxiv.org/pdf/1403.2965v1.pdf.
(61) Singh, V.; Bosman, S. J.; Schneider, B. H.; Blanter, Y. M.; Castellanos-Gomez, A.; Steele, G. A. Optomechanical coupling between a graphene mechanical resonator and a superconducting microwave cavity; arXiv preprint arXiv:1403.5165, 2014; http://arxiv.org/pdf/1403.5165v1.pdf.

■ NOTE ADDED IN PROOF

After submission of the manuscript, two related preprints appeared on the arXiv server (refs 60, 61).